A. B. Palazzolo

R. R. Lin

R. M. Alexander

Department of Mechanical Engineering,
Texas A&M University,
College Station, Texas 77843-3123

A. F. Kascak

J. Montague

ARMY-NASA Lewis Research Center,
MS 23/3,
Cleveland, Ohio 44135
Sverdrup Technology Inc.,
Middleburg Heights, Ohio 44130

Test and Theory for Piezoelectric Actuator-Active Vibration Control of Rotating Machinery

The application of piezoelectric actuators for active vibration control (AVC) of rotating machinery is examined. Theory is derived and the resulting predictions are shown to agree closely with results of tests performed on the air turbine driven-overhung rotor. The test results show significant reduction in unbalance, transient, and subsynchronous responses. Results from a 30 hour endurance test support the AVC system reliability. Various aspects of the electromechanical stability of the control system are also discussed and illustrated. Finally, application of the AVC system to an actual jet engine is discussed.

Introduction

Significant efforts are being made to apply active vibration control (AVC) devices to rotating machinery in the petrochemical, aerospace, and power utility industries. Advantages of AVC typically include adaptability to a myriad of load conditions, absence of lubrication systems with magnetic bearings, light weight, compactness, high or low temperature, etc.

Electromagnetic shakers and magnetic bearings have been used for actuators in the majority of the active vibration control research mentioned in the literature. Schweitzer (1985) and Ulbricht (1984) examined the stability and observability of rotor bearing systems with active vibration control, and presented an analysis which related force and stiffness to electrical and geometrical properties of electromagnetic bearings.

Nikolajsen (1979) examined the application of magnetic dampers to a 3.2 meter simulated marine propulsion system. Gondholekar and Holmes (1984) suggested that electromagnetic bearings be employed to shift critical speeds by altering the suspension stiffness. Wiese (1985) discussed proportional, integral, derivative (PID) control of rotor vibrations and illustrated how magnetic bearings could be used to balance a rotor by forcing it to spin about its inertial axis. Nonami (1986) presented theory for the active vibration control of rotor unbalance response by prescribing modal damping ratios. Humphris et al (1986) compared predicted and measured stiffness and damping coefficients for a magnetic journal bearing. Imlach et al (1988) presented a general design optimization scheme for selecting magnetic bearing design variables for particular applications. Kirk et al (1988) has discussed guidelines for achieving optimum rotor stability with magnetic bearings. Numerous other references on magnetic bearing can be found in the conference proceedings from the two previous references.

Several papers describe active vibration control utilizing

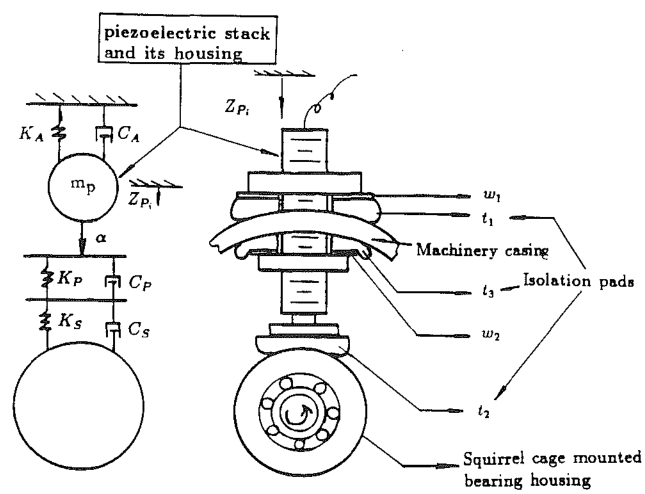

Horizontal

ω_1 (OD=50.8 mm)(ID=19.1 mm) t_1=8.13 mm t_2=5.08 mm
ω_2 (OD=50.8 mm)(ID=19.1 mm) t_3=4.57 mm

Vertical

ω_1 (OD=50.8 mm)(ID=19.1 mm) t_1=8.13 mm t_2=5.08 mm
ω_2 (OD=50.8 mm)(ID=19.1 mm) t_3=4.57 mm

Fig. 1 Idealized representation of the pusher and its connections

Contributed by the Technical Committee on Vibration and Sound for publication in the JOURNAL OF VIBRATION AND ACOUSTICS. Manuscript received August 1989; revised June 1990.

other types of actuators. Heinzmann (1980) employed loudspeaker coils linked to the shaft via ball bearings, to control vibrations. Feng (1986) developed an active vibration control scheme with actuator forces resulting from varying bearing oil pressure.

This paper develops theory and shows test results corresponding to incorporating piezoelectric pushers as actuator devices for active vibration control. The usual application for these devices is for obtaining minute position adjustments of lenses and mirrors in laser systems (Burleigh, 1986). In the proposed application the pushers force the squirrel cage-ball bearing supports of a rotating shaft. The paper presents active vibration control theory and test results for the piezoelectric pushers. The authors have previously presented some test results and an optimal control theory for piezoelectric pusher based AVC in Palazzolo et al (1988). The current paper extends this work by assuming that the pushers can be soft mounted to the machine case to improve electro-mechanical stability. In addition the experimental work in the previous paper was limited to sub-critical unbalance response, whereas super-critical unbalance response, transient vibration, and unstable vibrations are all shown to be controllable in experiments discussed in the current paper. To the authors' knowledge this represents a new application of piezoelectric actuators although there has been previous applications to the bending vibration of nonrotating beams using layered piezoelectric materials, i.e. Tzou (1987).

Theory

The piezoelectric pusher consists of a stack of piezoelectric ceramic discs which are arranged on top of one another and connected in parallel electrically. The stack expands in response to an applied voltage which causes the electric field to point in the direction of polarization for each disc. The extension of the pusher depends on the number and thickness of the discs and their piezoelectric charge constants (d_{33}). The force depends on the cross sectional area of the discs. Figure 1 shows a sketch of a pusher and the corresponding ideal model. The model consists of a prescribed displacement (α) which is assumed to be proportional to the input voltage, a lumped mass m_p which is constrained to move in the direction of the pusher, and a spring (K_P) representing the stiffness of the stack of piezoelectric discs. The parameters K_A, K_S, C_A, and C_S represent stiffnesses and dampings of isolation pads used to softmount the pushers. The model utilized in the upcoming analysis neglects nonlinearities in the electrical and structural characteristics of the devices in the piezoelectric stack.

If M pushers are forcing the rotor bearing system at its degrees of freedom $j_1, j_2, \ldots, j_M$, the matrix differential equation for the entire system may be rearranged into the form;

$$\begin{bmatrix} [M] & \vdots & [0] \\ \cdots & \cdots & \cdots \\ [0] & \vdots & [M_p] \end{bmatrix} \begin{Bmatrix} \{\ddot{\mathbf{Z}}\} \\ \cdots \\ \{\ddot{\mathbf{Z}}_p\} \end{Bmatrix} + \begin{bmatrix} [C'] & \vdots & [C''] \\ \cdots & \cdots & \cdots \\ [C'']^T & \vdots & [\hat{C}] \end{bmatrix} \begin{Bmatrix} \{\dot{\mathbf{Z}}\} \\ \cdots \\ \{\dot{\mathbf{Z}}_p\} \end{Bmatrix}$$

$$+ \begin{bmatrix} [K'] & \vdots & [K''] \\ \cdots & \cdots & \cdots \\ [K'']^T & \vdots & [\hat{K}] \end{bmatrix} \begin{Bmatrix} \{\mathbf{Z}\} \\ \cdots \\ \{\mathbf{Z}_p\} \end{Bmatrix} = \begin{Bmatrix} \{\mathbf{F}_D\} \\ \cdots \\ [0] \end{Bmatrix} + \begin{bmatrix} [-K''] & \vdots & [-C''] \\ \cdots & \cdots & \cdots \\ -[K_c] & \vdots & [-C_c] \end{bmatrix} \begin{Bmatrix} \{\alpha\} \\ \cdots \\ \{\dot{\alpha}\} \end{Bmatrix} \quad (1)$$

where N and M are the number of degrees of freedom of the rotor and the number of piezoelectric pushers, respectively. Note that vector $\{\mathbf{Z}\}$ is $N \times 1$ and vector $\{\mathbf{Z}_P\}$ is $M \times 1$. The matrices in equation (1) are defined by

Nomenclature

- ADFT = active damping feedback theory
- ASFT = active stiffness feedback theory
- AVC = active vibration control
- $[C]$ = damping matrix of the rotor without piezoelectric actuators
- $[C']$ = damping matrix of the rotor with passive (turned off) piezoelectric actuators installed
- $[C'']$ = matrix of passive damping coefficients between rotor and pusher dofs
- $[\hat{C}]$ = matrix of passive damping coefficients of the pushers
- $[\tilde{C}]$ = damping matrix of the rotor with active piezoelectric actuators
- C_{A_j} = passive damping of the pusher's soft mount
- C_c = $(1/C_s + 1/C_p)^{-1}$
- C_s = passive damping of isolator between piezo tip and bearing housing
- $\{\mathbf{F}_D\}$ = external forces (disturbances)
- $[G]$ = feedback gain matrix
- $[K]$ = stiffness matrix of the rotor without piezo actuators
- $[K']$ = stiffness matrix including the passive pusher stiffness
- $[K'']$ = passive stiffness matrix between rotor and pusher dofs
- $[\hat{K}]$ = passive stiffness matrix of the pushers
- K_a = passive stiffness of isolator between pusher and casing
- K_c = $(1/K_s + 1/K_p)^{-1}$
- K_p = passive stiffness of piezoelectric pusher
- K_s = passive stiffness of isolator between piezo tip and bearing housing
- L = total length of test shaft
- M = number of piezoelectric pushers
- m_j = mass of the jth pusher
- $[M]$ = mass matrix of the rotor
- $[M_p]$ = mass matrix of the pusher degrees of freedom
- $[\tilde{\tilde{M}}]$ = feedback mass matrix in ADFT
- N = number of degrees of freedom of the rotor
- $\{\mathbf{Z}\}$ = vector of rotor degrees of freedom
- $\{\mathbf{Z_P}\}$ = vector of pusher displacements (see Fig. 1)
- $\{\alpha\}$ = prescribed displacement of the pushers
- [diag( )] = diagonal matrix
- dof = degree of freedom

$$[M_p]_{(M\times M)} = [\mathrm{diag}(M_j)], \quad j=1, \ldots, M \tag{2}$$

$[C']_{(N\times N)}$

$$= [C]_{(N\times N)} + \begin{array}{c} \\ j_1 \\ j_2 \\ \\ j_m \\ \\ \end{array} \overset{\begin{array}{ccccccc} j_1 & \cdots & j_2 & \cdots & j_m & \cdots \end{array}}{\begin{bmatrix} \cdots & \vdots & \cdots & \vdots & \cdots & \vdots & \cdots \\ \cdots & C_{c1} & \cdots & \vdots & \cdots & \vdots & \cdots \\ \cdots & \vdots & \cdots & C_{c2} & \cdots & \vdots & \cdots \\ \cdots & \vdots & \cdots & \vdots & \ddots & \vdots & \cdots \\ \cdots & \vdots & \cdots & \vdots & \cdots & C_{cm} & \cdots \\ \cdots & \vdots & \cdots & \vdots & \cdots & \vdots & \cdots \end{bmatrix}} \tag{3}$$

$[C'']_{(N\times M)}$

$$= \begin{array}{c} \\ j_1 \\ j_2 \\ \\ j_m \\ \\ \end{array} \overset{\begin{array}{cccc} j_1 & j_2 & \cdots & j_m \end{array}}{\begin{bmatrix} \cdots & \cdots & \cdots & \cdots \\ -C_{c1} & \cdots & \cdots & \cdots \\ \cdots & -C_{c2} & \cdots & \cdots \\ \cdots & \cdots & \ddots & \cdots \\ \cdots & \cdots & \cdots & -C_{cm} \\ \cdots & \cdots & \cdots & \cdots \end{bmatrix}} \tag{4}$$

$$[\hat{C}]_{(M\times M)} = [\mathrm{diag}(C_{A_j} + C_{c_j})], \quad j=1, \ldots, M \tag{5}$$

$[K']_{(N\times N)}$

$$= [K]_{(N\times N)} + \begin{array}{c} \\ j_1 \\ j_2 \\ \\ j_m \\ \\ \end{array} \overset{\begin{array}{ccccccc} j_1 & \cdots & j_2 & \cdots & j_m & \cdots \end{array}}{\begin{bmatrix} \cdots & \vdots & \cdots & \vdots & \cdots & \vdots & \cdots \\ \cdots & K_{c1} & \cdots & \vdots & \cdots & \vdots & \cdots \\ \cdots & \vdots & \cdots & K_{c2} & \cdots & \vdots & \cdots \\ \cdots & \vdots & \cdots & \vdots & \ddots & \vdots & \cdots \\ \cdots & \vdots & \cdots & \vdots & \cdots & K_{cm} & \cdots \\ \cdots & \vdots & \cdots & \vdots & \cdots & \vdots & \cdots \end{bmatrix}} \tag{6}$$

$$[K'']_{(N\times M)} = \begin{array}{c} \\ j_1 \\ j_2 \\ \\ j_m \\ \\ \end{array} \overset{\begin{array}{cccc} j_1 & j_2 & \cdots & j_m \end{array}}{\begin{bmatrix} \cdots & \cdots & \cdots & \cdots \\ -K_{c1} & \cdots & \cdots & \cdots \\ \cdots & -K_{c2} & \cdots & \cdots \\ \cdots & \cdots & \ddots & \cdots \\ \cdots & \cdots & \cdots & -K_{cm} \\ \cdots & \cdots & \cdots & \cdots \end{bmatrix}} \tag{7}$$

$$[\hat{K}]_{(M\times M)} = [\mathrm{diag}(K_{A_j} + K_{c_j})], \quad j=1, \ldots, M \tag{8}$$

$$[C_c]_{(M\times M)} = [\mathrm{diag}(C_{c_j})], \quad j=1, \ldots, M \tag{9}$$

$$[K_c]_{(M\times M)} = [\mathrm{diag}(K_{c_j})], \quad j=1, \ldots, M \tag{10}$$

and

$$\{\alpha\} = \begin{Bmatrix} \alpha_1 \\ \alpha_2 \\ \vdots \\ \alpha_m \end{Bmatrix} \tag{11}$$

Note that in these definitions '. . .' indicates the presence of zeros. The matrices $[M]$, $[C]$, and $[K]$ are the mass, damping, and stiffness matrices of the rotor bearing system without the pushers installed, as defined in Palazzolo (1983). The matrix $[M_P]$ is the lumped mass matrix for the pushers. The K_{c_i} and C_{c_i} are the effective stiffness and damping between the pushers and the structure, which from Fig. 1 are $K_{c_i} = (1/K_{si} + 1/K_{pi})^{-1}$ and $C_{c_i} = (1/C_{si} + 1/C_{pi})^{-1}$. The stiffness K_{c_i} is inserted at the rotor degree of freedom which is in contact with the tip of the corresponding pusher. The K_{A_i} and C_{A_i} are the effective stiffness and damping between the pushers and the housing. The parameter α_i is the prescribed *internal* displacement of pusher i, which is assumed to vary linearly with input voltage. The "internal" displacement of the pusher is assumed to be approximately equal to the tip motion if the tip is not in contact with any resisting medium (i.e., a free tip).

The following portions of the paper present two AVC approaches incorporating the piezoelectric pusher model.

Part I: Active Damping Feedback Theory (ADFT)

Let the feedback law be defined as;

$$\{\alpha\}_{(M\times 1)} = -[G]_{(M\times N)}\{\dot{\mathbf{Z}}\}_{(N\times 1)} \tag{12}$$

where

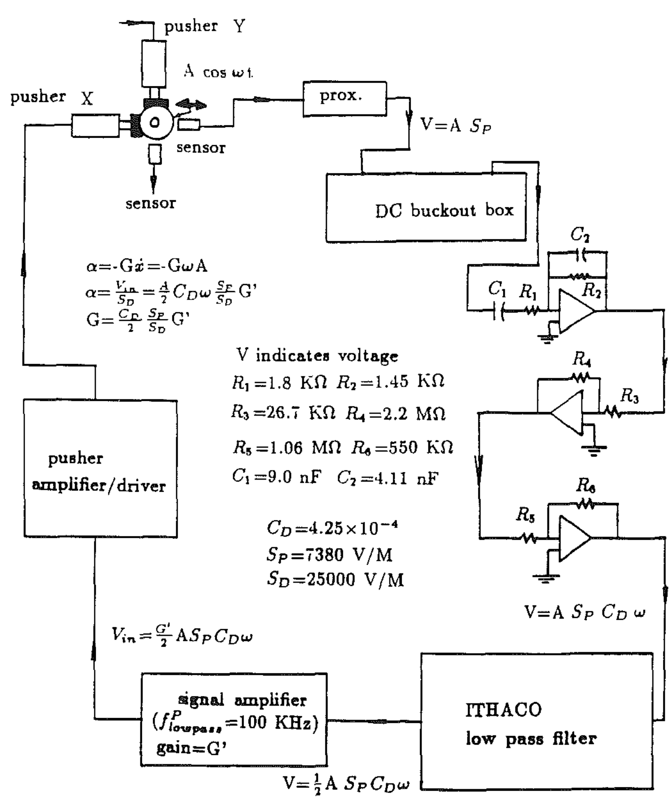

Fig. 2 Piezoelectric actuator based AVC system

$$
[G]_{(M\times N)} = \begin{array}{cc} & \begin{array}{cccccc} & j_1 & j_2 & \cdots & j_m & \end{array} \\ \begin{array}{c} 1 \\ 2 \\ \vdots \\ M \end{array} & \begin{bmatrix} \cdots & G_{11} & \cdots & \cdots & \cdots & \cdots \\ \cdots & \cdots & G_{11} & \cdots & \cdots & \cdots \\ \cdots & \cdots & \cdots & \ddots & \cdots & \cdots \\ \cdots & \cdots & \cdots & \cdots & G_{MM} & \cdots \end{bmatrix} \end{array} \tag{13}
$$

Substituting equation (12) and equation (13) into equation (1), gives the closed loop equation of the system;

$$
\begin{bmatrix} [\tilde{M}] & \vdots & [0] \\ \cdots & \cdots & \cdots \\ [\tilde{\tilde{M}}] & \vdots & [M_p] \end{bmatrix} \begin{Bmatrix} \{\ddot{\mathbf{Z}}\} \\ \cdots \\ \{\ddot{\mathbf{Z}}_p\} \end{Bmatrix} + \begin{bmatrix} [\tilde{C}_c] & \vdots & [C''] \\ \cdots & \cdots & \cdots \\ [\tilde{\tilde{C}}_c] & \vdots & [\hat{C}] \end{bmatrix} \begin{Bmatrix} \{\dot{\mathbf{Z}}\} \\ \cdots \\ \{\dot{\mathbf{Z}}_p\} \end{Bmatrix} + \begin{bmatrix} [K'] & \vdots & [K''] \\ \cdots & \cdots & \cdots \\ [K'']^T & \vdots & [\hat{K}] \end{bmatrix} \begin{Bmatrix} \{\mathbf{Z}\} \\ \cdots \\ \{\mathbf{Z}_p\} \end{Bmatrix} = \begin{Bmatrix} \{\mathbf{F}_D\} \\ \cdots \\ [0] \end{Bmatrix} \tag{14}
$$

$$
[\tilde{M}]_{(N\times N)} = [M]_{(N\times N)}
$$

$$
+ \begin{array}{cc} & \begin{array}{ccccccc} \cdots & j_1 & \cdots & j_2 & \cdots & \pi_\omega & \cdots \end{array} \\ \begin{array}{c} \\ j_1 \\ j_2 \\ \vdots \\ j_m \\ \vdots \end{array} & \begin{bmatrix} \cdots & \vdots & \cdots & \vdots & \cdots & \vdots & \cdots \\ \cdots & C_{c1}G_{11} & \cdots & \vdots & \cdots & \vdots & \cdots \\ \cdots & \vdots & \cdots & C_{c2}G_{22} & \cdots & \vdots & \cdots \\ \cdots & \vdots & \cdots & \vdots & \ddots & \vdots & \cdots \\ \cdots & \vdots & \cdots & \vdots & \cdots & C_{cm}G_{MM} & \cdots \\ \cdots & \vdots & \cdots & \vdots & \cdots & \vdots & \cdots \end{bmatrix} \end{array} \quad 15)
$$

$$
[\tilde{\tilde{M}}]_{(M\times N)} = \begin{array}{cc} & \begin{array}{cccccc} & j_1 & j_2 & \cdots & j_m & \end{array} \\ \begin{array}{c} 1 \\ 2 \\ \vdots \\ M \end{array} & \begin{bmatrix} \cdots & -C_{c1}G_{11} & \cdots & \cdots & \cdots & \cdots \\ \cdots & \cdots & -C_{c2}G_{22} & \cdots & \cdots & \cdots \\ \cdots & \cdots & \cdots & \ddots & \cdots & \cdots \\ \cdots & \cdots & \cdots & \cdots & -C_{cm}G_{MM} & \cdots \end{bmatrix} \end{array} \tag{16}
$$

$$
[\tilde{C}]_{(N\times N)} = [C] + \begin{array}{cc} & \begin{array}{ccccccc} \cdots & j_1 & \cdots & j_2 & \cdots & j_m & \cdots \end{array} \\ \begin{array}{c} \\ j_1 \\ j_2 \\ \vdots \\ j_m \\ \vdots \end{array} & \begin{bmatrix} \cdots & \vdots & \cdots & \vdots & \cdots & \vdots & \cdots \\ \cdots & (K_{c1}G_{11}+C_{c1}) & \cdots & \vdots & \cdots & \vdots & \cdots \\ \cdots & \vdots & \cdots & (K_{c2}G_{22}+C_{c2}) & \cdots & \vdots & \cdots \\ \cdots & \vdots & \cdots & \vdots & \ddots & \vdots & \cdots \\ \cdots & \vdots & \cdots & \vdots & \cdots & (K_{cm}G_{MM}+C_{cm}) & \cdots \\ \cdots & \vdots & \cdots & \vdots & \cdots & \vdots & \cdots \end{bmatrix} \end{array} \tag{17}
$$

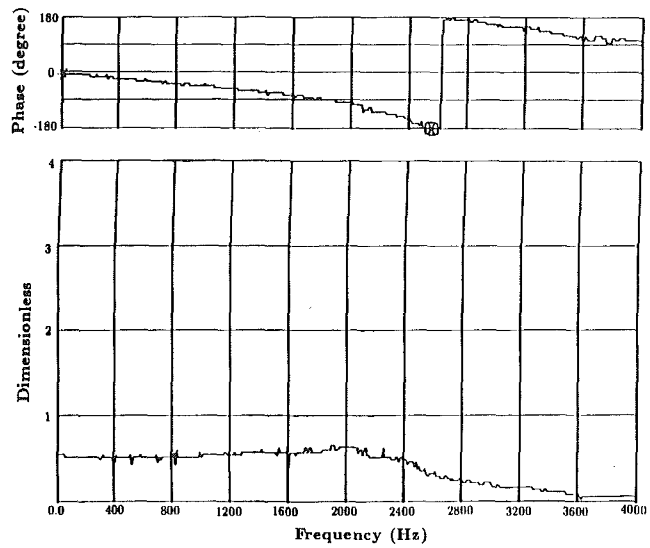

Fig. 3 Frequency response function of amplifier/driver for a piezoelectric pusher

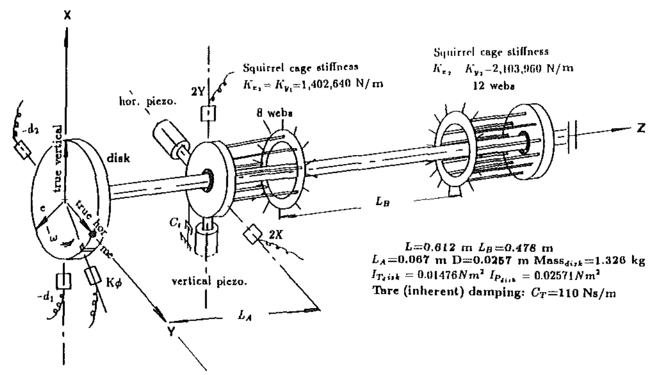

Fig. 4 Diagram of test rig with piezoelectric pushers

$$[\tilde{\tilde{C}}]_{(M\times N)} = \begin{array}{cc} & \begin{array}{cccccc} \quad & j_1 & \quad j_2 & \cdots & \quad j_m & \quad \end{array} \\ \begin{array}{c} 1 \\ 2 \\ \vdots \\ M \end{array} & \begin{bmatrix} \cdots & -(K_{c1}G_{11}+C_{c1}) & \cdots & \cdots & \cdots & \cdots \\ \cdots & \cdots & -(K_{c2}G_{22}+C_{c2}) & \cdots & \cdots & \cdots \\ \cdots & \cdots & \cdots & \ddots & \cdots & \cdots \\ \cdots & \cdots & \cdots & \cdots & -(K_{cm}G_{MM}+C_{cm}) & \cdots \end{bmatrix} \end{array} \qquad (18)$$

Part II: Active Stiffness Feedback Theory (ASFT)

In this section, the pusher internal displacements are proportional to the rotor displacements rather than to the rotor velocities. The feedback control law is;

$$\{\alpha\}_{(M\times 1)} = -[G]_{(M\times N)}\{\mathbf{Z}\}_{(N\times 1)} \qquad (19)$$

Note that the feedback gain matrix $[G]$ is defined in equation (13). Substituting equation (19) and equation (13) into equation (1), gives the closed-loop system equation as;

$$\begin{bmatrix} [M] & \vdots & [\mathbf{0}] \\ \cdots & \cdots & \cdots \\ [\mathbf{0}] & \vdots & [M_p] \end{bmatrix} \begin{Bmatrix} \{\ddot{\mathbf{Z}}\} \\ \cdots \\ \{\ddot{\mathbf{Z}}_p\} \end{Bmatrix} + \begin{bmatrix} [\tilde{C}_K] & \vdots & [C''] \\ \cdots & \cdots & \cdots \\ [\tilde{\tilde{C}}_K] & \vdots & [\hat{C}] \end{bmatrix} \begin{Bmatrix} \{\dot{\mathbf{Z}}\} \\ \cdots \\ \{\dot{\mathbf{Z}}_p\} \end{Bmatrix}$$

$$+ \begin{bmatrix} [\tilde{K}] & \vdots & [K''] \\ \cdots & \cdots & \cdots \\ [\tilde{\tilde{K}}] & \vdots & [\hat{K}] \end{bmatrix} \begin{Bmatrix} \{\mathbf{Z}\} \\ \cdots \\ \{\mathbf{Z}_p\} \end{Bmatrix} = \begin{Bmatrix} \{\mathbf{F}_D\} \\ \cdots \\ [0] \end{Bmatrix} \qquad (20)$$

Note that the matrix $[G]$ has the same form for both ADFT and ASFT, but the units are different. In ADFT, the unit of $[G]$ is in sec while the $[G]$ in ASFT is dimensionless.

Test Results and Theory Comparison

A series of component and system tests were performed in order to stabilize the AVC system, verify its effectiveness in controlling vibration, and verify the theory presented. Figure 2 shows the feedback loop used for the velocity feedback (damping) tests. The circuit shown in this figure contains a differentiator, amplifier, and inverter. The position feedback (stiffness) test loop was identical except for removal of the resistors, capacitors, and operational amplifiers shown.

The dimensions of the various components of the pusher assembly are shown in Fig. 1. The isolation pads are neoprene compression pads (Tech Products, 1988). The pushers are shown to be soft mounted or isolated from the metal housing utilizing neoprene pads in Fig. 1.

The pads were found to improve the electromechanical

$$[\tilde{C}_K]_{(N\times N)} = [C] + \begin{bmatrix} \cdots & \vdots & \cdots & \vdots & \cdots & \vdots & \cdots \\ \cdots & C_{c1}(1+G_{11}) & \cdots & \vdots & \cdots & \vdots & \cdots \\ \cdots & \vdots & \cdots & C_{c2}(1+G_{22}) & \cdots & \vdots & \cdots \\ \cdots & \vdots & \cdots & \vdots & \ddots & \vdots & \cdots \\ \cdots & \vdots & \cdots & \vdots & \cdots & C_{cm}(1+G_{MM}) & \cdots \\ \cdots & \vdots & \cdots & \vdots & \cdots & \vdots & \cdots \end{bmatrix} \qquad (21)$$

$$[\tilde{\tilde{C}}_K]_{(M\times N)} = \begin{array}{cc} & \begin{array}{cccccc} \quad & j_1 & \quad j_2 & \cdots & \quad j_m & \quad \end{array} \\ \begin{array}{c} 1 \\ 2 \\ \vdots \\ M \end{array} & \begin{bmatrix} \cdots & -C_{c1}(1+G_{11}) & \cdots & \cdots & \cdots & \cdots \\ \cdots & \cdots & -C_{c2}(1+G_{22}) & \cdots & \cdots & \cdots \\ \cdots & \cdots & \cdots & \ddots & \cdots & \cdots \\ \cdots & \cdots & \cdots & \cdots & -C_{cm}(1+\mathrm{G_{MM}}) & \cdots \end{bmatrix} \end{array} \qquad (22)$$

$$[\tilde{K}]_{(N\times N)} = [K] + \begin{bmatrix} \cdots & \vdots & \cdots & \vdots & \cdots & \vdots & \cdots \\ \cdots & K_{c1}(1+G_{11}) & \cdots & \vdots & \cdots & \vdots & \cdots \\ \cdots & \vdots & \cdots & K_{c2}(1+G_{22}) & \cdots & \vdots & \cdots \\ \cdots & \vdots & \cdots & \vdots & \ddots & \vdots & \cdots \\ \cdots & \vdots & \cdots & \vdots & \cdots & K_{cm}(1+G_{MM}) & \cdots \\ \cdots & \vdots & \cdots & \vdots & \cdots & \vdots & \cdots \end{bmatrix} \qquad (23)$$

$$[\tilde{\tilde{K}}]_{(M\times N)} = \begin{array}{cc} & \begin{array}{cccccc} \quad & j_1 & \quad j_2 & \cdots & \quad j_m & \quad \end{array} \\ \begin{array}{c} 1 \\ 2 \\ \vdots \\ M \end{array} & \begin{bmatrix} \cdots & -K_{c1}(1+G_{11}) & \cdots & \cdots & \cdots & \cdots \\ \cdots & \cdots & -K_{c2}(1+G_{22}) & \cdots & \cdots & \cdots \\ \cdots & \cdots & \cdots & \ddots & \cdots & \cdots \\ \cdots & \cdots & \cdots & \cdots & -K_{cm}(1+\mathrm{G_{MM}}) & \cdots \end{bmatrix} \end{array} \qquad (24)$$

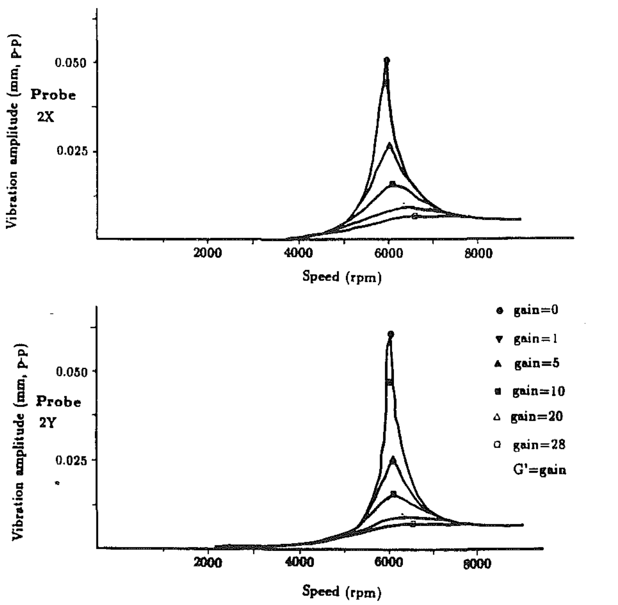

Fig. 5 Response amplitude at probes 2X and 2Y in Fig. 4 vs. feedback gain

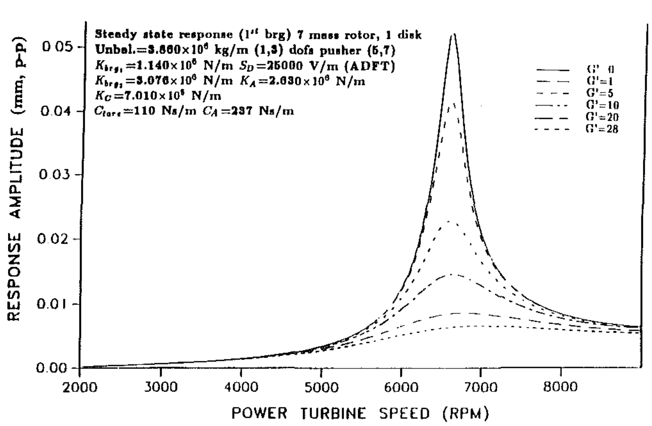

Fig. 6 Simulation unbalance response at probe 2X or 2Y in Fig. 4 vs. feedback gain coefficient in ADFT.

stability of the system. The reason for this is that introducing flexibility in the casing-pusher connection point reduced vibration of the casing. This prevents out of phase motion of the pusher support point which may cause instability. The trade off in this action is that the pusher forces are reduced, yet, as evidenced by the test results, remain effective over a certain range of feedback gains for the system examined. The absorber pads introduce passive damping which also enhances the stability.

Figure 2 is a diagram of the feedback control system. The differentiator yields a frequency response function proportional to frequency to about 1000 Hz where it rolls off to prevent high frequency noise amplification. The roll off introduces phase lag which tends to destabilize the system. The low pass filter was inserted to attenuate high frequency noise, but again introduces phase lag. The most significant phase lag comes from the pusher and its driver, which like all other actuators rolls off in amplitude above some frequency. Figure 3 shows the frequency response function between the pusher's amplifier/driver input voltage and its output voltage to the pusher. Note that although the amplitude is flat to 2000 Hz, considerable phase lag does occur. The frequency response function between the pusher's tip displacement and its input voltage is very similar to Fig. 3 but slightly less damped.

Figure 4 shows a sketch of the test rig at NASA Lewis Research Center, including probe and pusher locations. The

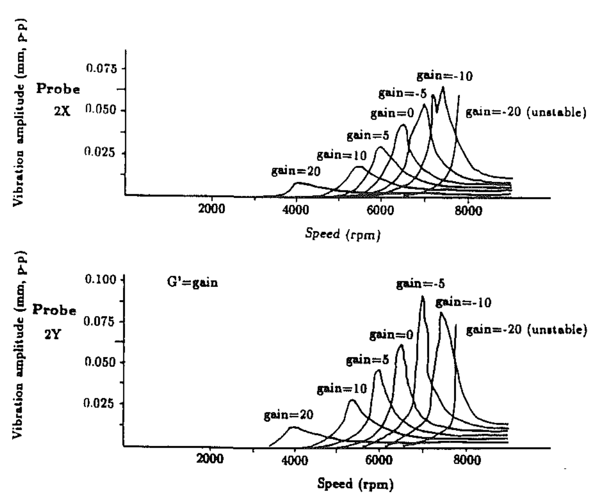

Fig. 7 Response amplitude at probes 2X and 2Y in Fig. 4 vs. gain in ASFT

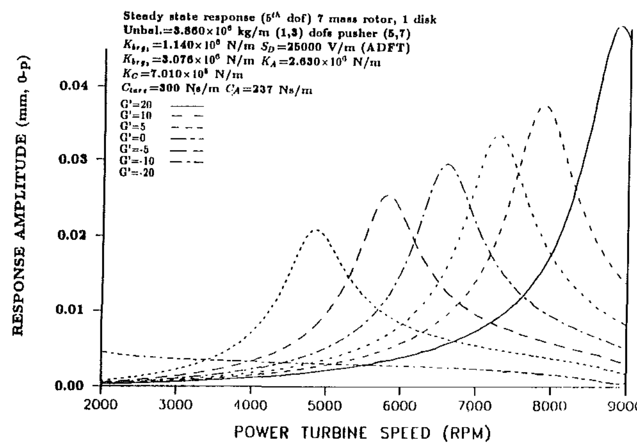

Fig. 8 Simulation unbalance response at probe 2X or 2Y in Fig. 4 vs. feedback gain coefficient in ASFT

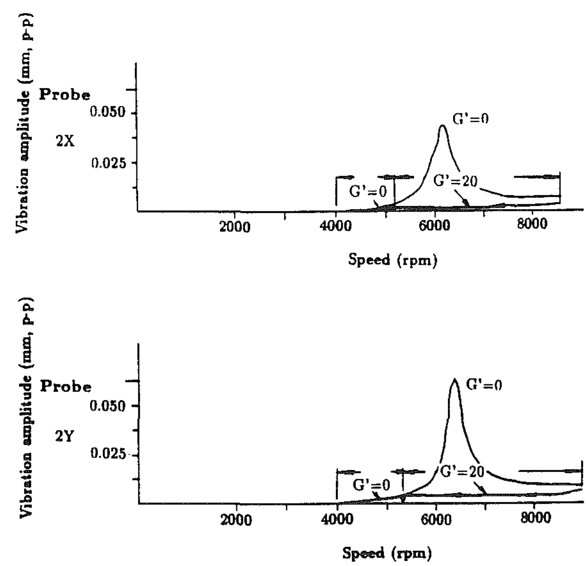

Fig. 9 Demonstration of coastdown vibration reduction by switching critical speed location

rotor was simulated with a 7 mass finite element model including the active damping and stiffness matrices derived in the analysis section. The active damping theoretical feedback gain coefficient [G_{ii} in equation (13)] is obtained from Fig. 2 as

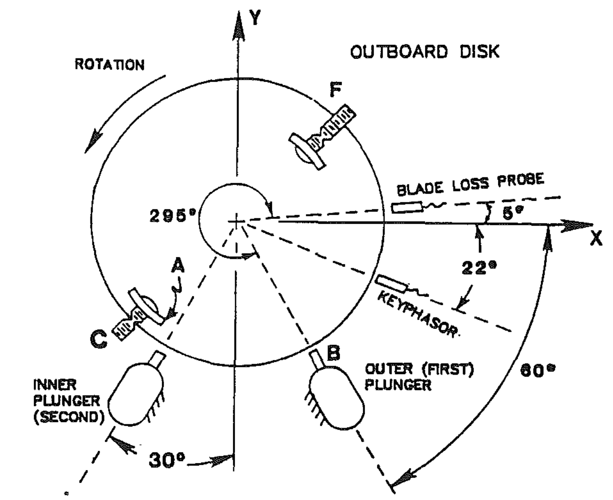

Fig. 10 Sudden mass imbalance device at outboard disc location

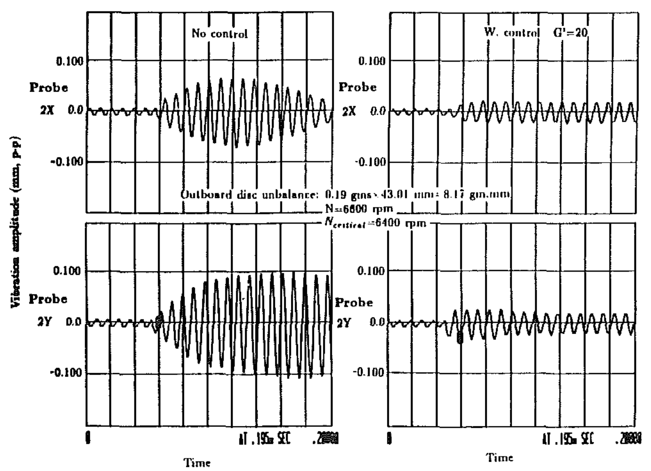

Fig. 11 Experimental transient response-sudden bolt loss

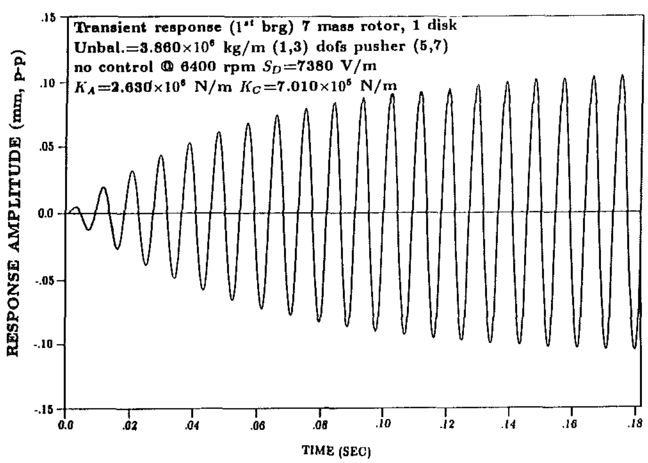

Fig. 12 Simulation transient response to sudden mass unbalance-no velocity feedback

$$G_{ii} = \frac{C_D S_P}{2 \times S_D} G'_{ii} \tag{25}$$

The pusher's passive damping C_p and the damping C_s of the absorber between the pusher tip and the bearing housing were neglected. This resulted in the active "mass" matrices in equation (15) and equation (16) to be null for this study. The following response plots show displacement vibration at

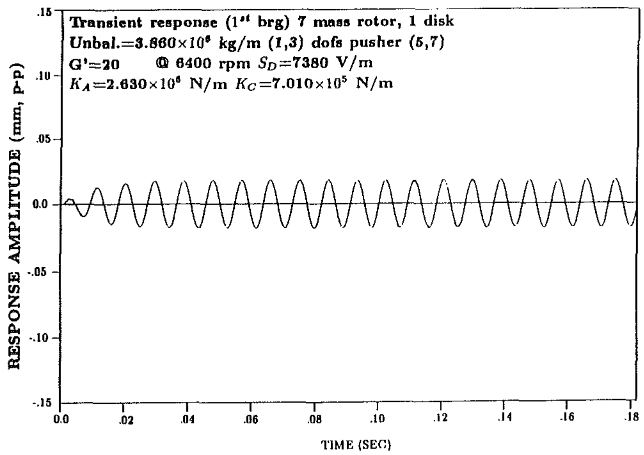

Fig. 13 Simulation transient response to sudden mass unbalance-with velocity feedback control (G' = 20)

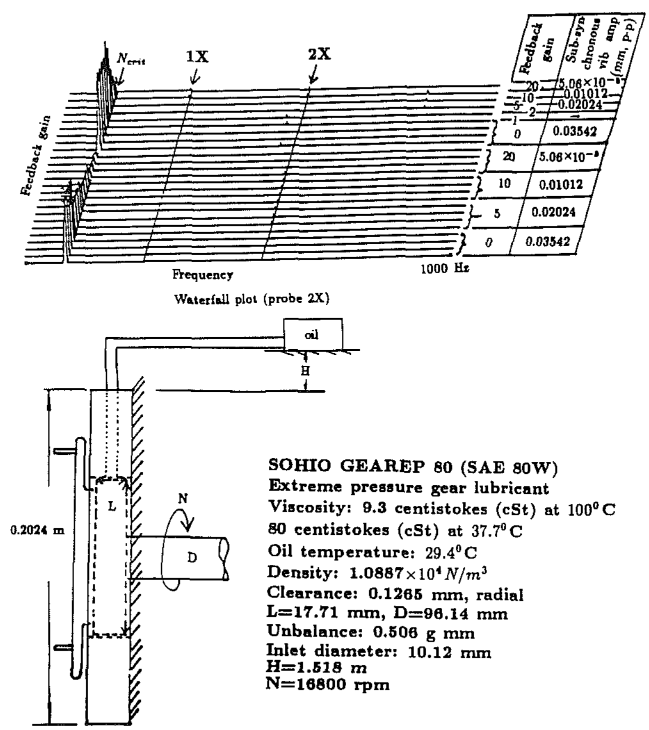

Fig. 14 Oil whirl suppression test: N = 16800 rpm

probes $2X$ and $2Y$ in this figure. The effects of varying the signal amplifier gain G' in the active damping circuit of Fig. 2 is shown in the unbalance response plots of Fig. 5. These results show close agreement with the theoretical response plot shown in Fig. 6. The theoretical feedback gain coefficient is obtained from the instrument sensitivities and amplifier gain G' as shown in Fig. 2. The tare (inherent passive) damping was found to be 110 N sec/m which was obtained by test/simulation matching. This damping was applied between the bearing housing and ground in both transverse directions.

Test results for active stiffness are shown in Fig. 7. The response curves in these figures shown the effect that feedback gain has on the critical speed location. Figure 8 shows the corresponding theoretical predictions for various values of feedback gain in the active stiffness circuit. Note that the active stiffness may raise or lower the critical speed depending on the sign of the feedback, which is experimentally controlled by an inverter circuit. Furthermore, since C_p and C_s are neglected the matrices in equations (21) and (22) are both null. The abili-

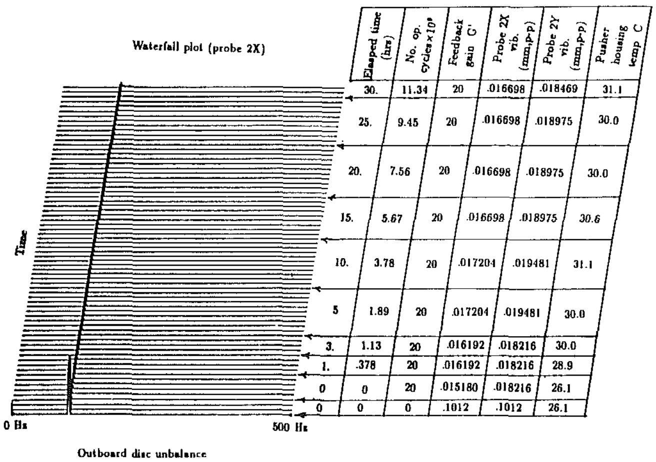

Fig. 15 **Durability test with the rotor speed at critical speed: 6300 rpm**

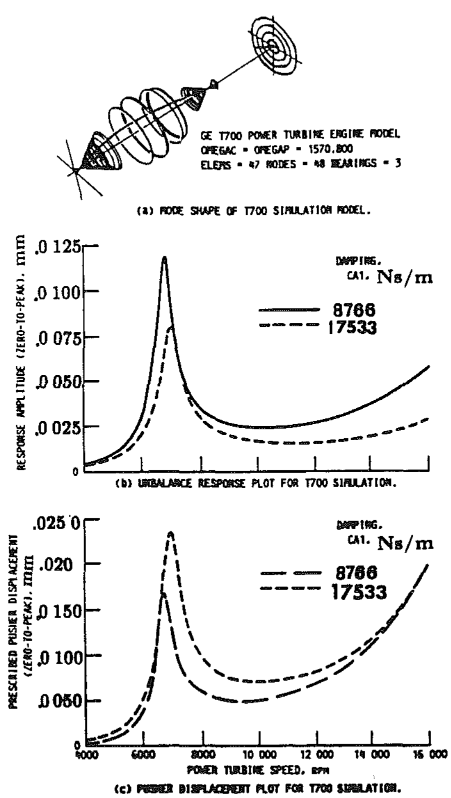

Fig. 16 **T700 engine simulation results**

ty of active stiffness to shift critical speeds can be exploited to avoid resonance during runup or coastdown. This is illustrated in Fig. 9 where $G' = -20$ at 8500 rpm and is switched during coastdown to 0 at 5500 rpm, thus avoiding a major resonance peak. This can be clearly understood by considering the $G' = 20$ and $G' = 0$ curves in Fig. 8.

A transient "sudden" weight loss test was conducted by shearing off a bolt with a solenoid driven plunger as shown in Fig. 10. A complete description of the test procedure and apparatus may be found in Kascak (1987). Figure 11 shows the measured response during the transient without velocity feedback (active damping) and with velocity feedback at gain $G' = 20$. Figures 12 and 13 show the corresponding theoretical responses using Newmark Beta ($\alpha = 0.25$ $\delta = 0.5$) numerical integration.

The velocity feedback AVC was tested to see if it could successfully stop instability. Figure 14 shows how the outboard disk was used as a plane journal bearing to induce an instability from oil whirl. The figure indicates that the rotor was balanced very well, displaying only a minute vibration component at running speed (N). The waterfall plot shows frequency spectrums of the probe ($2X$) vibration signal versus velocity feedback gain. The instability frequency is at the 6100 rpm critical speed ($N_{crit.}$) while the rotor operating speed is 16800 rpm. Increasing the velocity feedback gain decreased the subsynchronous component of vibration by a factor of 7.

Finally, Fig. 15 shows the results of a 30 hour (11.0×10^6 cycles) endurance test of the velocity feedback AVC loop. The plot shows a waterfall spectrum of the displacement vibration at the $2X$ location in Fig. 4. The rotor speed was set equal to the critical speed and the active damping given was set equal to $G' = 20$ during this test. The results indicate excellent vibration reduction throughout the test. This removed some initial fears that the pushers would become ineffective in long duration operation due to self heating. Piezoelectric actuators behave like capacitors with a small amount of dielectric loss that produces some power dissipation or self-heating in the device when driven at high amplitudes and high frequency. Evidently the low vibration amplitude and frequency prevented this effect.

Electromechanical Stability

The system described in this paper has electromechanical stability limitations. The reasons for these limitations are the phase lags of the differentiator circuit, low pass filter, piezoelectric pusher, and its drivers as shown in Fig. 2. The differentiator circuit was designed to have the minimum possible phase lag without permitting its rolloff frequency to be so high as to severely amplify noise. In addition, the low pass filter cutoff frequency was adjusted to be as low as possible, to attenuate high frequency noise, without introducing too severe a phase lag which may cause electromechanical instability. The pusher's driver has a built in low pass filter on its output. This filter's feedback capacitor was adjusted to minimize its phase lag and improve electromechanical stability.

For accurate prediction of electromechanical stability for the system described here it is required to represent the differentiator, low pass filter, pusher, and its driver with linear differential equations. These equations may be written for the differentiator and the low pass filter from a standard circuit's textbook. The pusher and its driver must first be represented by equivalent circuits with similar frequency response functions. The frequency response function between the pusher tip's free (unconstrained) displacement and the input voltage to the pusher is very important since it provides a more realistic model for α in Fig. 1, which was previously assumed to be proportional to the pusher's input voltage and without phase lag. Our tests show that the frequency response functions of these components are very similar to those of *2nd* and 4th order low pass filters. Correlation of instability onset gains with an analytical model utilizing the equivalent circuit representation has shown very encouraging results. This analysis and results are quite extensive and are summarized in Lin (1990).

Simulation of Actual Jet Engine

Computer simulations were performed to determine the force and stroke requirements of the piezoelectric pushers for active damping application in a typical jet engine. For these simulations it was assumed that the pushers were hard mounted to the casing, i.e., $K_A = C_A = \infty$ in Fig. 1, and that they were located in both transverse directions at the exhaust bearing of the power turbine shaft.

Figure 16 shows the first mode, and unbalance response and pusher internal displacement (α) plots for a T700 type turbine engine. The T700 falls in the category, "Small General Aviation Engine (SGAE)," according to criteria proposed in Bhat (1983);

	Max. Rotor Weight (Newton)	Max. Rotor Length (Meter)	Max. Speed RPM
SGAE	667.50	1.777	20,000
T700	93.45	0.964	16,000 (service)

A comparison of the T700 results to the maximum acceptable vibration proposed in the Bhat report is shown below:

	Max. Turbine Vibration at Operating Speed (Meter, 0-p)/g mm	Max. Damper Vibration at Operating Speed (Meter, 0-p)/g mm
SGAE	1.76×10^{-7}	1.59×10^{-7}
T700	2.47×10^{-8}	1.76×10^{-8}

The T700 results are for an active damper ($K_{c_i}G_{ii}$) value of 17533 Newton. sec/m (100 lb sec/in) which requires a pusher internal displacement of 2.03×10^{-4} meters, zero to peak (8.0 mils) for 72.0 gm cm (1 oz in) unbalance at the turbine disc. The corresponding pusher force is 890 Newtons (200 lbs, zero to peak). Although the pusher displacement requirement exceeds the $5.06\times10^{-5}-7.59\times10^{-5}$ meter (zero to peak) limit of existing pushers, larger displacements can be obtained by stacking piezo-pushers in series. Similar simulations are currently being performed on the T64 and T55 engines.

Summary and Conclusions

This paper presented theory, test results, and comparisons for utilizing piezoelectric pushers as actuators for active control of rotor bearing system vibrations. The results showed that the velocity feedback AVC could effectively suppress unbalance response, transient, and subsynchronous vibrations. The control system successfully suppressed unbalance induced vibrations throughout a 30 hour endurance test. The active stiffness AVC was effective in positioning the critical speed in order to avoid resonance during startup or coastdown speed transients.

Correlation between unbalance response test and theory showed very good agreement for velocity feedback AVC and fair agreement for position feedback AVC. Future work in this area will examine high and low temperature performance, developing pushers with more force and stroke, and improving electromechanical stability for application to actual industrial and aerospace machinery.

Acknowledgments

The authors wish to express their sincere gratitude for the following funding sources: NASA grant NAG3-763, ASEE-NASA Summer Faculty Fellowship Program, the U.S. Army at NASA Lewis, and the Texas A&M Turbomachinery Research Consortium (TRC). The invaluable assistance of the following people is also gratefully acknowledged: NASA (Jerry Brown, Al DiRusso, Tom Lakatos, Erwin Meyn, and John Ropchock), Burleigh, Inc., (Dr. Jim Kaufer, Lance Portland, Louis Rapp, Roger Greenwald), and Texas A&M University (Drs. Mooring and Jayasuriya).

References

Bhat, S. T., et al., 1983, "Analysis of High Load Dampers," NASA CR165503, PWA 5779-10.

Burleigh Instruements, Burleigh Park, Fishers, NY, 14453.

Burleigh, 1988, "The Piezo Book," 330-288-51683-0, Burleigh Park, Fishers, NY, 14453.

Feng, G., Xin, N., 1986, "Automatic Control of the Vibration of the Flexible Rotor with Microcomputer," Int. Conf. on Rotordynamics, IFTOMM and JSME, Tokyo, Sept., pp. 14-17.

Gondholekar, V., and Holmes, R., 1984, "Design of Electromagnetic Bearing for Vibration Control of Flexible Transmission Shaft," Rotor Dynamic Instability Problem in High Performance Turbomachinery, Texas A&M Univ., NASA report.

Heinzmann, J., et al., 1980, "The Implementation of Automatic Vibration Control in a High Speed Rotating Test Facility," Univ. of Virginia Report UVA/464761/MAE80/160.

Humphris, R., et al., 1986, "Effect of Control Algorithms on Magnetic Journal Bearing Properties," ASME *Journal of Engineering Turbines and Power*, Oct., Vol. 108, pp. 624-632.

Imlach, J., Allaire, P., Humphris, R., and Barrett, L., 1988, "Magnetic Bearing Design Optimization," *Proceedings of the Inter. Conf. on Vibrations in Rotating Machinery, Proc. of Inst. of Mech. Eng.*, Herriot-Watt Univ., Edinburgh, Scotland.

Kascak, A., Palazzolo, A., and Montaque, G., 1987, "Transient Rotor Dynamic Rub Phenomena, Theory and Test," ASME De-Vol. 2, Rotating Machinery Dynamics, pp. 485-494.

Kirk, R., Hustak, J., and Schoeneck, K., 1988, "Analysis and Test Results of Two Centrifugal Compressors Using Active Magnetic Bearings," *Proceedings of the Inter. Conf. on Vibrations in Rotating Machinery, Proc. of Inst. of Mech. Eng.*, Herriot-Watt Univ., Edinburgh, Scotland.

Lin, R. R., Palazzolo, A. B., Kascak, A., Montague, G., 1990, "Electro-Mechanical Simulation of Actively Controlled Rotordynamic Systems with Piezoelectric Actuators," The *6th* Workshop on Rotordynamic Instability Problems in High-Performance Turbomachinery, Texas A&M University, May.

Nikolajsen, J., Holmes, R., and Gondholekar, V., 1979, "Investigation of an Electromagnetic Damper for Vibration Control of a Transmissionn Shaft," *Proc. Instn. Mech. Engr.*, Vol. 193, pp. 331-336.

Nonami, K., 1985, "Vibration Control of Rotor Shaft System by Active Control Bearings," ASME Vibration Conf., Cincinnati, 1985, Paper No. 85-DET-126.

Palazzolo, A. B., Wang, B. P., and Pilkey, W. D., 1983, "Eigensolution Reanalysis of Rotordynamic Systems by the Generalized Receptance Method," ASME *Journal of Engineering for Power*, Vol. 105, July, pp. 543-550.

Palazzolo, A. B., Lin, R. R., Kascak, A. F., and Alexander, R. M., 1988, "Active Control of Transient Rotordynamic Vibration by Optimal Control Methods," Paper No. 88-GT-73, Presented at Gas Turbine Conf., June 5-9, 1988, Amsterdam, ASME *Journal of Engineering for Gas Turbine and Power*, April 1989.

Palazzolo, A., Kascak, A., Lin, R. R., and Montague, J., 1988, "Piezoelectric Pushers for Active Control of Rotating Machinery Vibrations," Fifth Workshop on Rotordynamic Instability, Texas A&M Univ., Sponsored by NASA.

Schweitzer, G., 1985, "Magnetic Bearings for Vibration Control," Bently Nevada Instability Seminar, Minden, Nevada.

Tech Products Corporation, 1988, "Noise and Vibration Control Products," Catalog 876, Dayton, Ohio.

Tzou, H. S., 1987, "Active Vibration Control of Flexibel Structures Via Converse Piezoelectricity," Presented at the 20th Midwestern Mechanics Conference, 8/31-9/2, 1987, Developments in Mechanics, pp. 1201-1206, Vol. 14-c.

Ulbricht, H., and Anton, E., 1984, "Theory and Application of Magnetic Bearing with Integrated Displacement and Velocity Sensors," I. Mech. E. Conf. on Rotordynamics, Paper C 299/84.

Weise, D., 1985, "Active Magnetic Bearings Provide Closed Loop Servo Control for Enhanced Dynamic Response," Proc. *27th* IEEE Machine Tool Conf., October.